Improved endurance capacity of diabetic mice during SGLT2 inhibition: Role of AICARP, an AMPK activator in the soleus

中村，慎太郎

KYUSHU UNIVERSITY

Improved endurance capacity of diabetic mice during SGLT2 inhibition: Role of AICARP, an AMPK activator in the soleus

Shintaro Nakamura[1], Yasutaka Miyachi[1]* [ID], Akihito Shinjo[1], Hisashi Yokomizo[1], Masatomo Takahashi[2], Kohta Nakatani[2], Yoshihiro Izumi[2], Hiroko Otsuka[1], Naoichi Sato[1], Ryuichi Sakamoto[1], Takashi Miyazawa[1], Takeshi Bamba[2] & Yoshihiro Ogawa[1]*

[1]*Department of Medicine and Bioregulatory Science, Graduate School of Medical Sciences, Kyushu University, Fukuoka, Japan;* [2]*Division of Metabolomics/Mass Spectrometry Center, Medical Research Center for High Depth Omics, Medical Institute of Bioregulation, Kyushu University, Fukuoka, Japan*

Abstract

Background   Diabetes is associated with an increased risk of deleterious changes in muscle mass and function or sarcopenia, leading to physical inactivity and worsening glycaemic control. Given the negative energy balance during sodium–glucose cotransporter-2 (SGLT2) inhibition, whether SGLT2 inhibitors affect skeletal muscle mass and function is a matter of concern. However, how SGLT2 inhibition affects the skeletal muscle function in patients with diabetes remains insufficiently explored. We aimed to explore the effects of canagliflozin (CANA), an SGLT2 inhibitor, on skeletal muscles in genetically diabetic *db/db* mice focusing on the differential responses of oxidative and glycolytic muscles.

Methods   *Db/db* mice were treated with CANA for 4 weeks. We measured running distance and handgrip strength to assess skeletal muscle function during CANA treatment. At the end of the experiment, we performed a targeted metabolome analysis of the skeletal muscles.

Results   CANA treatment improved the reduced endurance capacity, as revealed by running distance in *db/db* mice (414.9 ± 52.8 vs. 88.7 ± 22.7 m, $P < 0.05$). Targeted metabolome analysis revealed that 5-aminoimidazole-4-carboxamide-1-β-D-ribofuranosyl 5′-monophosphate (AICARP), a naturally occurring AMP-activated protein kinase (AMPK) activator, increased in the oxidative soleus muscle ($P < 0.05$), but not in the glycolytic extensor digitorum longus muscle ($P = 0.4376$), with increased levels of AMPK phosphorylation ($P < 0.01$).

Conclusions   This study highlights the potential role of the AICARP/AMPK pathway in oxidative rather than glycolytic skeletal muscles during SGLT2 inhibition, providing novel insights into the mechanism by which SGLT2 inhibitors improve endurance capacity in patients with type 2 diabetes.

Keywords   AICARP; AMPK; endurance exercise; fatty acid oxidation; SGLT2 inhibitor; skeletal muscle

Introduction

Sarcopenia, characterized by reduced skeletal muscle mass and strength, is associated with increased adverse outcomes, including falls, fractures and mortality.[1] The causes of sarcopenia include ageing, malnutrition and chronic diseases, such as cancer and diabetes. Diabetes may affect the distribution and metabolism of muscle fibres. Previous studies showed a

reduced proportion of myosin heavy chain (MyHC) type I oxidative muscle fibres and an increased proportion of type II glycolytic muscle fibres in patients with type 2 diabetes.[2]

In general, type I fibres have lower fatigability and higher oxidative capacity than type II fibres; thus, an increase in type I fibres may improve endurance performance in long-distance running.[3] Exercise can improve the oxidative capacity of skeletal muscle[4] and induce a fibre-type switch from type II to type I,[5] suggesting skeletal muscle plasticity. By contrast, physical inactivity and reduced exercise capacity have been observed in patients with diabetes.[6,7] The reduced oxidative enzyme activity in the skeletal muscle from patients with type 2 diabetes can be reversed by thiazolidinedione treatment.[8] However, the effects of oral glucose-lowering drugs on skeletal muscle metabolism and function in patients with diabetes have not been intensively investigated.

Sodium–glucose cotransporter-2 (SGLT2) inhibitors are oral glucose-lowering drugs that promote the urinary excretion of glucose by blocking its reabsorption in the renal proximal tubules. SGLT2 inhibition results in a negative energy balance, indicating that SGLT2 inhibitors also affect skeletal muscle metabolism and function.[9] Specifically, SGLT2 inhibition improves exercise endurance capacity by enhancing fatty acid (FA) oxidation in the skeletal muscle of mice with heart failure.[10] We previously reported the differential metabolic effects of canagliflozin (CANA), an SGLT2 inhibitor, on slow oxidative and fast glycolytic skeletal muscles in normoglycaemic mice, which was affected by the amount of food intake.[11] These observations suggest that the metabolic effect of SGLT2 inhibitors on skeletal muscle depends on glucose availability. Several studies have reported that SGLT2 inhibitors can improve the endurance capacity of streptozotocin (STZ)-induced hyperglycaemic mice.[12,13] However, there is no detailed analysis of how SGLT2 inhibitors affect skeletal muscle metabolism in obese diabetic mice focusing on the differential responses of oxidative and glycolytic muscles. Thus, this study aimed to explore the effects of CANA on oxidative and glycolytic skeletal muscles in genetically diabetic db/db mice.

Methods

Animals and experimental protocols

All experimental protocols were approved by the Committee on Ethics of Animal Experiments at Kyushu University (No. A21-062-2). Male C57BLKS/J Iar-+Leprdb/+Leprdb (db/db) and C57BLKS/J Iar-m+/+Leprdb (db/+) mice were purchased from Charles River Laboratories Japan, Inc. (Yokohama, Japan). All mice were housed in a pathogen-free facility and maintained on a 12-h light and 12-h dark cycle with free access to normal chow diet (CRF-1, Oriental Yeast Co., Ltd., Tokyo, Japan) and water. CANA (Mitsubishi Tanabe Pharma

Corporation, Osaka, Japan) was mixed at 0.03% (w/w) with CRF-1 and administered to 8-week-old db/+ and db/db mice for 4 weeks. Food intake was calculated for three consecutive days each week using the mouse feeder MF-4S (Shin Factory, Fukuoka, Japan) as previously described.[11] Body weight and random blood glucose levels were monitored once a week during the experiments. At the end of the experiments, 6-h-fasted mice were anaesthetized with isoflurane and blood samples were obtained from the inferior vena cava. Skeletal muscles including soleus and extensor digitorum longus (EDL), epididymal and subcutaneous white adipose tissues (eWAT and sWAT, respectively), and liver were immediately frozen and stored at −80°C unless otherwise noted.

Metabolic analysis

Blood glucose and serum insulin levels were measured using Stat Strip XP3 (Nipro, Osaka, Japan) and enzyme-linked immunosorbent assay (ELISA) (Morinaga Institute of Biological Science, Yokohama, Japan), respectively. For intraperitoneal glucose tolerance test (ipGTT), mice were fasted for 16 h with free access to water and then intraperitoneally injected with glucose (2 g/kg). For insulin tolerance test (ITT), 5-h-fasted db/db mice were intraperitoneally injected with human insulin (0.5 U/kg). Blood glucose was measured at 0, 15, 30, 60, 90 and 120 min after glucose or insulin injection, and serum insulin levels were measured at 0, 15 and 30 min after glucose injection.

Measurement of endurance capacity and grip strength

A treadmill exercise test was performed using Ratbelt-2000 (Arco System, Chiba, Japan) as previously described to measure endurance capacity.[11] Mice were acclimated for 4–5 days prior to the exercise test. The test consisted of three sessions beginning at a rate of 12 m/min for 40 min. After the initial session, the speed was increased by 1 m/min every 10 min for 30 min. After the second session, the speed was increased by 1 m/min every 5 min until exhaustion, which was defined as the point at which the mice stopped running despite gentle taps on the back. Grip strength was measured using MK-380CM/R (Muromachi Kikai, Tokyo, Japan) as previously described.[11] The highest maximum force among the five trials was recorded.

Quantitative real-time PCR analysis

Total RNA was extracted from the muscle, and cDNA was synthesized as previously described.[11] Primer sequences are listed in Table S1. The mRNA levels were normalized to those of 18S mRNA.

Histology

The muscle tissues were mounted on cork supports using gum tragacanth (Sigma-Aldrich, Munich, Germany) and embedded in optimal cutting temperature compound. Frozen sections (12 μm) were air-dried and fixed with 4% paraformaldehyde in phosphate-buffered saline (PBS) for 5 min. For the quantification of muscle fibre cross-sectional area, fixed sections were incubated for 1 h at 4°C with Alexa Fluor 488-conjugated wheat germ agglutinin (Invitrogen, MA, USA) in PBS at 1:1000 dilution. For the analysis of MyHC isoforms, immunohistochemical staining was performed as previously described.[11]

Cell culture

C2C12 cells (CRL-1772, ATCC) were maintained in Dulbecco's modified Eagle's medium (DMEM) with 4.5-g/L glucose containing 10% foetal bovine serum and penicillin–streptomycin. Cells were treated with CANA for 24 h. For knockdown experiments, cells were transfected with an siRNA-targeting adenylosuccinate lyase (ADSL, s62087, Thermo Fisher Scientific, MA, USA) or a scrambled sequence (4390843, Invitrogen) using Lipofectamine RNAiMAX (Thermo Fisher Scientific). After 24-h incubation, ADSL knockdown cells were treated with CANA for an additional 24 h.

Western blot analysis

The muscle tissues were homogenized in radioimmunoprecipitation assay (RIPA) buffer containing protease inhibitor cocktail (Nacalai Tesque, Kyoto, Japan) and phosphatase inhibitors (PhosSTOP, Roche, Basel, Switzerland). Samples were separated by sodium dodecyl sulfate–polyacrylamide gel electrophoresis (SDS-PAGE) using 4–15% gradient gels (Bio-Rad, CA, USA) and transferred to polyvinylidene difluoride (PVDF) membranes. Immunoblotting was performed using anti-PKM1 (7067, Cell Signaling Technology [CST], MA, USA), anti-PKM2 (4053, CST), anti-phospho-acetyl-CoA carboxylase (ACC) (3661, CST), anti-ACC (3662, CST), anti-β-actin (sc-1616, Santa Cruz Biotechnology, TX, USA), anti-ADSL (sc-365623, Santa Cruz Biotechnology), anti-SGLT2 (ab37296, Abcam, Cambridge, UK), anti-carnitine palmitoyltransferase 1A (CPT1A) (12252, CST), anti-phospho-AMP-activated protein kinase α (AMPKα) (2535, CST) and anti-AMPKα (2532, CST) antibodies. All primary antibodies were used at 1:1000 dilution, except for β-actin (1:5000).

Thiobarbituric acid reactive substances assay

The muscle tissues were homogenized in RIPA buffer containing protease inhibitor cocktail. Samples were analysed using thiobarbituric acid reactive substances (TBARS) assay kit (Cayman Chemical, MI, USA). TBARS levels were normalized to total protein concentrations.

Targeted metabolome analysis

Skeletal muscle and serum samples were prepared for metabolite extraction using the Bligh and Dyer method[14] with minor modifications.[11] Briefly, metabolites were extracted from frozen and crushed skeletal muscle (~10 mg) or serum (20 μL) with 1 mL of solvent mixture (methanol:chloroform: water = 10:4:4, v/v/v) containing piperazine-1,4-bis(2-ethanesulfonic acid) (PIPES) (0.63 μmol/L), 2-bromohypoxanthine (0.13 μmol/L), free FA 16:0 ($^{13}C_{16}$) (0.13 μmol/L), diacylglycerol (DG) 15:0–18:1 (d_7) (0.15 μmol/L) and triacylglycerol (TG) 15:0–18:1 (d_7) –15:0 (0.35 μmol/L) as internal standards. The samples were vigorously mixed for 1 min and sonicated for 5 min. The extracts were then centrifuged at 16 000 × g for 5 min at 4°C, and the resultant supernatant was collected. Protein concentrations in the pellets were determined using a Pierce™ BCA Protein Assay Kit (Thermo Fisher Scientific). The collected supernatant (700 μL) was mixed with 235 μL of chloroform, and 155 μL of water, and then centrifuged at 16 000 × g for 5 min at 4°C.

The aqueous (upper) layer (400 μL) was transferred to a clean tube for an ion chromatography (Dionex ICS-5000⁺ HPIC System, Thermo Fisher Scientific) with a Dionex IonPac AS11-HC-4 mm column (2-mm i.d. × 250 mm, 4-μm particle size, Thermo Fisher Scientific) coupled with a Q Exactive, high-performance benchtop quadrupole Orbitrap high-resolution tandem mass spectrometer (Thermo Fisher Scientific; IC/MS) for targeted anionic polar metabolites (e.g., organic acids, sugar phosphates and nucleotides),[15] a liquid chromatography (Nexera X2 UHPLC System, Shimadzu Co., Kyoto, Japan) with a Discovery HS F5 column (2.1-mm i. d. × 150 mm, 3-μm particle size, Merck, Darmstadt, Germany) coupled with a Q Exactive instrument (PFPP-LC/MS) for targeted cationic polar metabolites (e.g., amino acids, bases and nucleosides)[15] and an LC (Shimadzu Co.) with a metal-free peek-coated InertSustain C18 column (2.1-mm i.d. × 150 mm, 3-μm particle size, GL Sciences Inc., Tokyo, Japan) coupled with a Q Exactive instrument (C18-LC/MS) for acetyl-CoA, acyl-CoAs and acyl-carnitines.[15] After the aqueous layer extracts were evaporated under vacuum, dried extracts were stored at −80°C until use for targeted polar metabolome analysis using IC/MS, PFPP-LC/MS and C18-LC/MS. Prior to analysis, the dried aqueous layer was reconstituted in 50 μL of water. Identification of the hydrophilic metabolites was accomplished by comparing retention time and MS and MS/MS spectra of the samples with those of authentic standards analysed under identical conditions using an in-house library.[15]

The organic (lower) layer (200 μL) was transferred to a clean tube for a supercritical fluid chromatography (SFC, Nexera UC System, Shimadzu Co.) with an ACQUITY UPC^2 HSS C18 column (3.0-mm i.d. × 100 mm, 1.8-μm particle size, Waters, MA, USA) coupled with a triple quadrupole mass spectrometry (TQMS, LCMS-8060, Shimadzu Co.) (C18-SFC/MS/MS) for FAs[15] and an SFC (Shimadzu Co.) with an ACQUITY UPC^2 Torus diethylamine (DEA; 3.0-mm i.d. × 100 mm, 1.7-μm particle size, Waters) coupled with a TQMS (DEA-SFC/MS/MS) for DGs and TGs.[15,16] After the organic layer extracts were dried under a nitrogen stream, dried extracts were stored at −80°C until use for targeted lipidome analysis using C18-SFC/MS/MS and DEA-SFC/MS/MS. Prior to analysis, the organic aqueous layer was reconstituted in 80 μL of methanol/chloroform (1/1, v/v). Identification of lipids was conducted based on the retention time and precursor ion, and the fragmentation patterns or specific multiple reaction monitoring transitions of each molecule.[15,16] Tables S2 and S3 list the abbreviations of the hydrophilic and hydrophobic metabolites, respectively. Data analysis was performed using MetaboAnalyst 5.0 (https://www.metaboanalyst.ca/). To exclude the effect of exercise and external nutrients other than regular diet on metabolites in skeletal muscles, we analysed soleus and EDL muscles from 6-h-fasted mice that were not challenged with exercise tests.

Statistical analysis

All data were analysed using GraphPad Prism 8 and are expressed as the mean ± SEM. Statistical analysis was performed using Student's *t* test or one-way analysis of variance (ANOVA) with Fisher's protected least significant difference test. Two-way ANOVA followed by Šidák's multiple comparison test was used to examine the influence of two different variables. $P < 0.05$ was considered statistically significant.

Data availability

The raw metabolomics data have been deposited into the Metabolomics Workbench (https://www.metabolomicsworkbench.org/) under study ID of ST002729.

Results

Changes in body composition and glucose metabolism

We administered CANA to male *db*/+ and *db*/*db* mice for 4 weeks (Figure 1A). CANA treatment normalized the blood glucose levels in *db*/*db* mice (Figure 1B) without affecting body weight and food consumption (Figure 1C,D). CANA treatment decreased the weight of liver and eWAT in *db*/*db* mice (Figure S1A,B), while sWAT weight was unchanged (Figure S1C).

To assess glucose metabolism in CANA-treated *db*/*db* mice, we performed ipGTT. CANA treatment decreased the area under the curve (AUC) of ipGTT and serum insulin concentration at 30 min during ipGTT (Figures 1E and S1D). Consistently, the AUC of ITT was lower in CANA-treated *db*/*db* mice than in control *db*/*db* mice without CANA treatment (Figure 1F).

Effects of SGLT2 inhibition on skeletal muscle mass and function

We next assessed the muscle mass of *db*/+ and *db*/*db* mice. Obese hyperglycaemic mice showed an ~30% decrease in muscle mass of the soleus, a representative oxidative muscle, compared with normoglycaemic mice (Figure 2A). The fibre size of soleus muscle also reduced in *db*/*db* mice (Figure 2A). CANA treatment did not affect the weight and fibre size of soleus muscle from *db*/*db* mice (Figure 2A). We also observed similar changes in the weights and fibre sizes of EDL (Figure 2B), glycolytic muscle and quadriceps femoris (Figure S1E). By contrast, CANA treatment attenuated the weight reduction of gastrocnemius and tibialis anterior muscles in *db*/*db* mice (Figure S1F,G).

To determine the effects of CANA treatment on muscle function, we evaluated the running distance and handgrip strength of CANA-treated *db*/*db* mice. The running distances of 8-week-old *db*/*db* mice were impaired relative to those of the age-matched *db*/+ mice, with a marked difference at 12 weeks of age (Figure 2C). Four-week CANA treatment increased ~5-fold running distance in *db*/*db* mice (Figure 2C, D). By contrast, there was no significant difference in grip strength between *db*/+ and *db*/*db* mice with and without CANA treatment (Figure 2E,F).

Considering that SGLT2 inhibition enhanced the endurance capacity in *db*/*db* mice, we hypothesized that CANA treatment would affect muscle fibre composition in soleus muscle. Soleus muscle is mostly composed of MyHC types I and IIa, both of which are oxidative fibres,[17] whereas EDL muscle is rich in glycolytic fibres, types IIb and IIx.[17] In this study, we found an increased proportion of type IIx in soleus muscle from *db*/*db* mice, but this increase was attenuated by CANA treatment (Figure S2A). By contrast, there were no appreciable changes in fibre composition in EDL, gastrocnemius and tibialis anterior muscles (Figure S2B–D).

Targeted metabolome analysis of skeletal muscles

To explore the metabolic changes that may account for the functional difference in the oxidative and glycolytic muscles
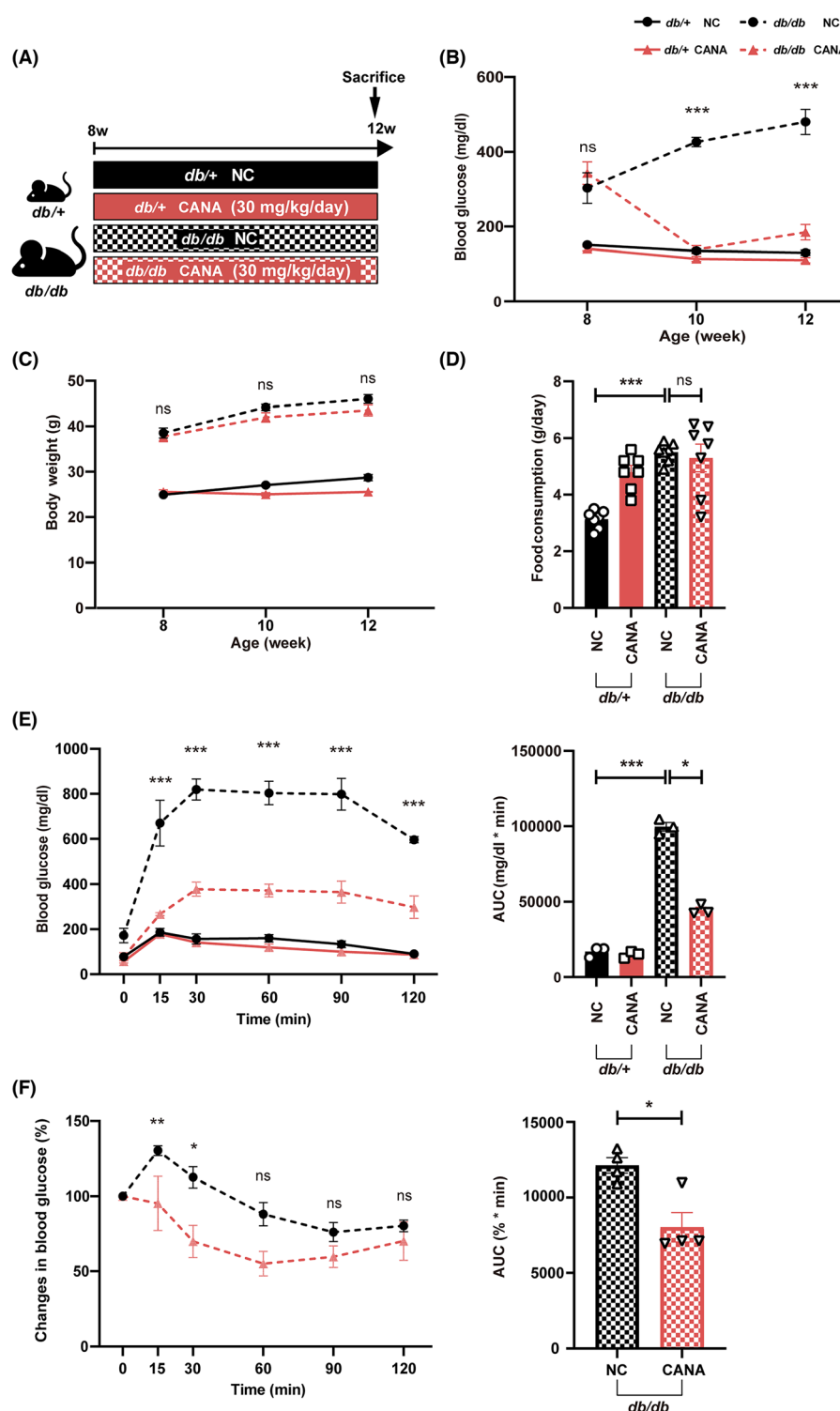
Figure 1 Changes in body weight and glucose metabolism during sodium–glucose cotransporter-2 (SGLT2) inhibition. (A) Animal experimental protocol. Male 8-week-old *db/+* and *db/db* mice were fed with normal chow (NC) or canagliflozin (CANA)-containing diet for 4 weeks. Changes in random blood glucose levels (B) and body weight (C) during CANA treatment ($n = 7$). (D) Average daily food intake at 4 weeks of CANA treatment ($n = 7$). (E) Intraperitoneal glucose tolerance test (ipGTT) (1 g/kg) at 3 weeks of CANA treatment ($n = 3$). Area under the curve (AUC) of ipGTT. (F) Insulin tolerance test (ITT) (0.5 U/kg) at 3 weeks of CANA treatment and AUC of ITT ($n = 4$). Y axis indicates the percentage changes in blood glucose from baseline (0 min). Data are presented as the mean ± SEM. Group difference was assessed using one-way analysis of variance (ANOVA) in (D) and (E) (AUC of ipGTT) or two-way ANOVA in (B), (C) and (E) (ipGTT) and (F) (ITT). *$P < 0.05$, **$P < 0.01$ and ***$P < 0.001$ versus CANA-treated *db/db* mice. ns, not significant.
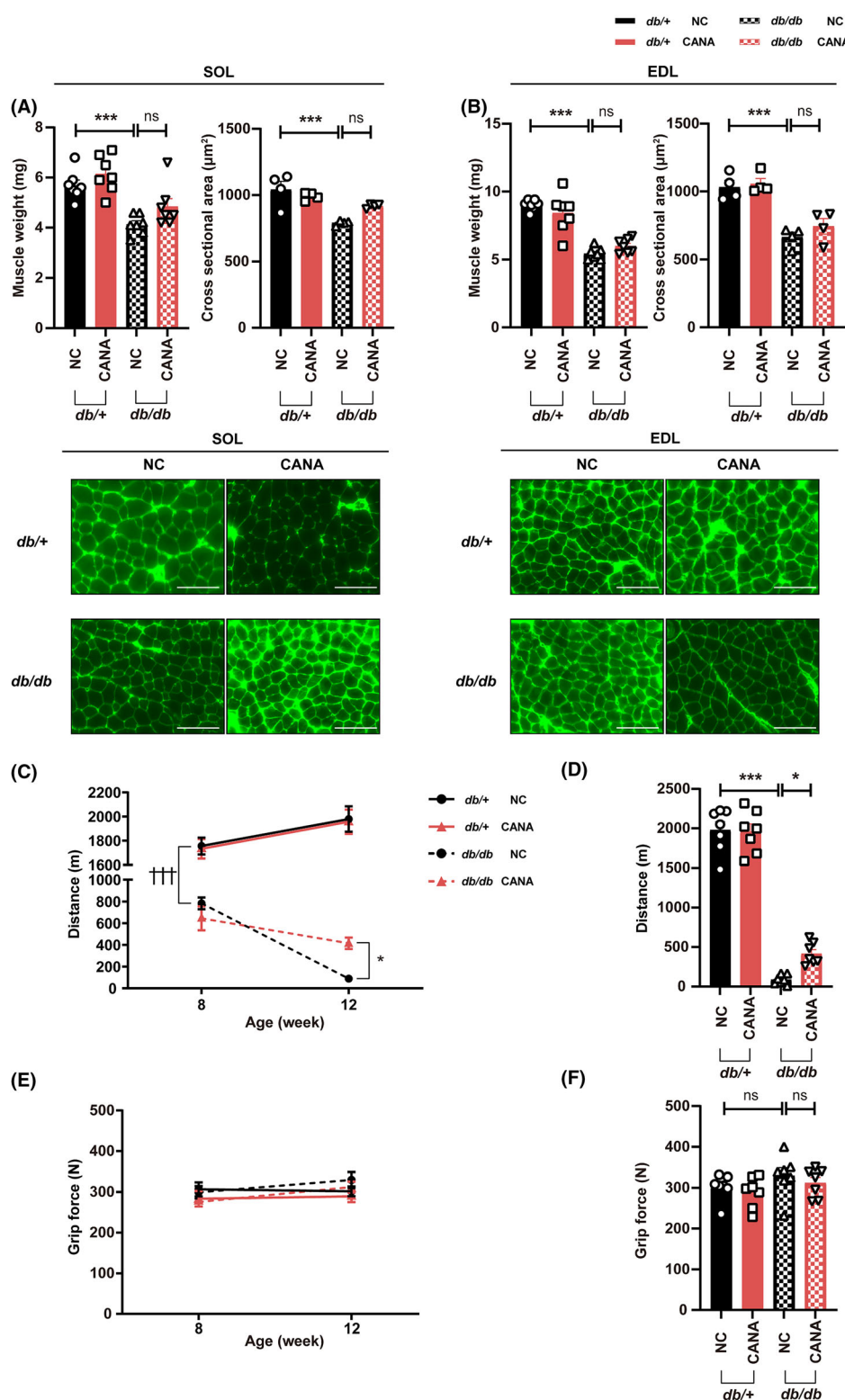
Figure 2 Effect of sodium–glucose cotransporter-2 (SGLT2) inhibition on skeletal muscle weight and function. Lower limb muscle weight (upper left), cross-sectional area (upper right) and representative wheat germ agglutinin staining of muscle fibres (lower) in soleus (SOL) (A) and extensor digitorum longus (EDL) muscles (B). Scale bar = 100 μm. (C–F) Running distance assessed by treadmill exercise test and grip strength. Changes in distance (C) and grip strength (E) during canagliflozin (CANA) treatment. Distance (D) and grip strength (F) at 4 weeks of CANA treatment. Data are expressed as the mean ± SEM. Group difference was assessed using one-way analysis of variance (ANOVA) in (D) and (F) or two-way ANOVA in (C) and (E). *$P < 0.05$, **$P < 0.01$ and ***$P < 0.001$. $^{†††}P < 0.001$ versus control $db/+$ mice. ns, not significant.

from CANA-treated *db/db* mice, we performed a targeted metabolome analysis of skeletal muscles from *db/db* mice with and without CANA treatment and *db/+* mice as a reference.

Overall, 217 and 218 hydrophilic metabolites were identified in soleus and EDL muscles, respectively (*Figure 3A* and *Table S2*). Pathway analysis revealed marked changes in lipid metabolism (e.g., sphingolipids and FAs) in soleus muscle, whereas amino acid metabolism was altered in soleus and EDL muscles by CANA treatment (*Figure 3B*). Moreover, CANA treatment upregulated four and six metabolites by more than two-fold in the soleus and EDL muscles from *db/db* mice, respectively (*Figure 3C*). Among those upregulated in the soleus, 5-aminoimidazole-4-carboxamide-1-β-D-ribofuranosyl 5'-monophosphate (AICARP) was upregulated only in soleus muscle, whereas *N*-acetyl-ornithine and hydroxybutyric acid including 2-hydroxybutyric acid were upregulated in soleus and EDL muscles. Regarding hydroxybutyric acid, 3-hydroxybutyric acid was upregulated in soleus muscle (*Figure S3A*). We also identified four metabolites including hexose (i.e., glucose), which were downregulated in soleus muscle after CANA treatment; all of these metabolites were downregulated in EDL muscle.

Metabolites of glycolysis and tricarboxylic acid cycle in skeletal muscles

Insulin resistance is associated with increased intramuscular lipid levels.[18] In this study, soleus muscle from *db/db* mice showed ~4-fold and ~2-fold higher TG and DG levels, respectively, than those of *db/+* mice (*Figure S3B* and *Table S3*). We also found that TG and DG accumulated in EDL muscle from *db/db* mice (*Figure S3C*). Acetyl-CoA and intermediates of the tricarboxylic acid (TCA) cycle decreased in soleus muscle, suggesting that lipid metabolism was dysregulated in skeletal muscles from *db/db* mice (*Figure S3D*). By contrast, acetyl-CoA levels increased ~2-fold in EDL muscle, accompanied by increases in glucose-6-phosphate (G6P) and fructose-6-phosphate (F6P), both of which are intermediates of glycolysis (*Figure S3C,E*). Given that EDL muscle is rich in type IIb and IIx fibres that generate ATP via anaerobic glycolysis, acetyl-CoA is derived mostly from pyruvate; however, pyruvate levels decreased in EDL muscle from *db/db* mice (*Figure S3C*).

Skeletal muscles produce energy using carbohydrates and FAs as fuels. To evaluate the metabolic effect of CANA treatment on skeletal muscles, we compared the metabolites of glycolysis and the TCA cycle in soleus and EDL muscles from CANA-treated and control *db/db* mice. CANA treatment decreased glucose levels in soleus and EDL muscles by 50% (*Figure 4A,B*). By contrast, CANA treatment increased acetyl-CoA levels in soleus muscle by 60%, in parallel with an increase in FAs (*Figure 4A,C*). In addition, CANA treatment

increased citrate and aconitate levels by ~40%, and isocitrate, succinate and fumarate levels by nearly 50%, suggesting an overall increase in the metabolites of the TCA cycle (*Figure 4C*). We also found a two-fold increase in intermediates of glycolysis such as G6P and F6P in soleus muscle after CANA treatment (*Figure 4A*). However, CANA treatment only slightly affected the metabolites of glycolysis and the TCA cycle in EDL muscle (*Figure 4B,D*).

To further evaluate glycolysis in soleus and EDL muscles, we measured mRNA expression of rate-limiting enzymes in the glycolytic pathway: hexokinase 2 (HK2), phosphofructokinase (PFKM), pyruvate kinase muscle isozyme (PKM) and pyruvate dehydrogenase alpha (PDHα) (*Figure S4A*). CANA treatment did not affect gene expression of HK2, PFKM and PDHα but upregulated that of PKM1, which converts phosphoenolpyruvate to pyruvate in the final step of the glycolytic pathway, in soleus muscle from *db/db* mice (*Figure S4B*). Therefore, we examined the amount of PKM1 and another isoform of PKM, PKM2, in soleus and EDL muscles. PKM1 protein expression decreased in soleus muscle from *db/db* mice, but this phenomenon was reversed by CANA treatment (*Figure S4C*). We observed minimal changes in PKM1 expression in EDL muscle and PKM2 expression in soleus and EDL muscles (*Figure S4D*).

Changes in fatty acid β-oxidation in oxidative soleus muscle

FA oxidation in skeletal muscle is impaired in patients with type 2 diabetes.[19] In this study, *db/db* mice showed the accumulation of long-chain acyl-CoAs (C12–C18) in soleus muscle, whereas CANA treatment increased the levels of medium- and short-chain acyl-CoAs, such as acetyl-CoA (*Figure 5A*). We obtained similar data for acyl-carnitines in soleus muscle (*Figure 5B*). Conversely, acyl-CoAs showed no consistent trends in EDL muscle, with the accumulation of medium-chain acyl-CoAs (C8–C10) in *db/db* mice (*Figure 5C*). By contrast, the levels of acyl-carnitines except for acetylcarnitine were higher in EDL muscle from *db/+* mice than in that from *db/db* mice (*Figure 5D*).

Carnitine palmitoyltransferase 1 (CPT1) is a key enzyme for FA oxidation and is involved in the transport of long-chain FAs into the mitochondria (*Figure 5E*). In this study, CPT1 expression was slightly decreased in soleus muscle from *db/db* mice but was unaffected in soleus and EDL muscles from CANA-treated *db/db* mice (*Figure 5F*). ACC is also involved in FA synthesis and oxidation,[20] thereby catalyzing acetyl-CoA into malonyl-CoA in skeletal muscle (*Figure 5E*). Phosphorylation of ACC was reduced in soleus muscle from *db/db* mice, suggesting dysregulation of FA β-oxidation (*Figure S5A*). CANA treatment did not affect ACC phosphorylation in soleus and EDL muscles (*Figure S5A,B*).
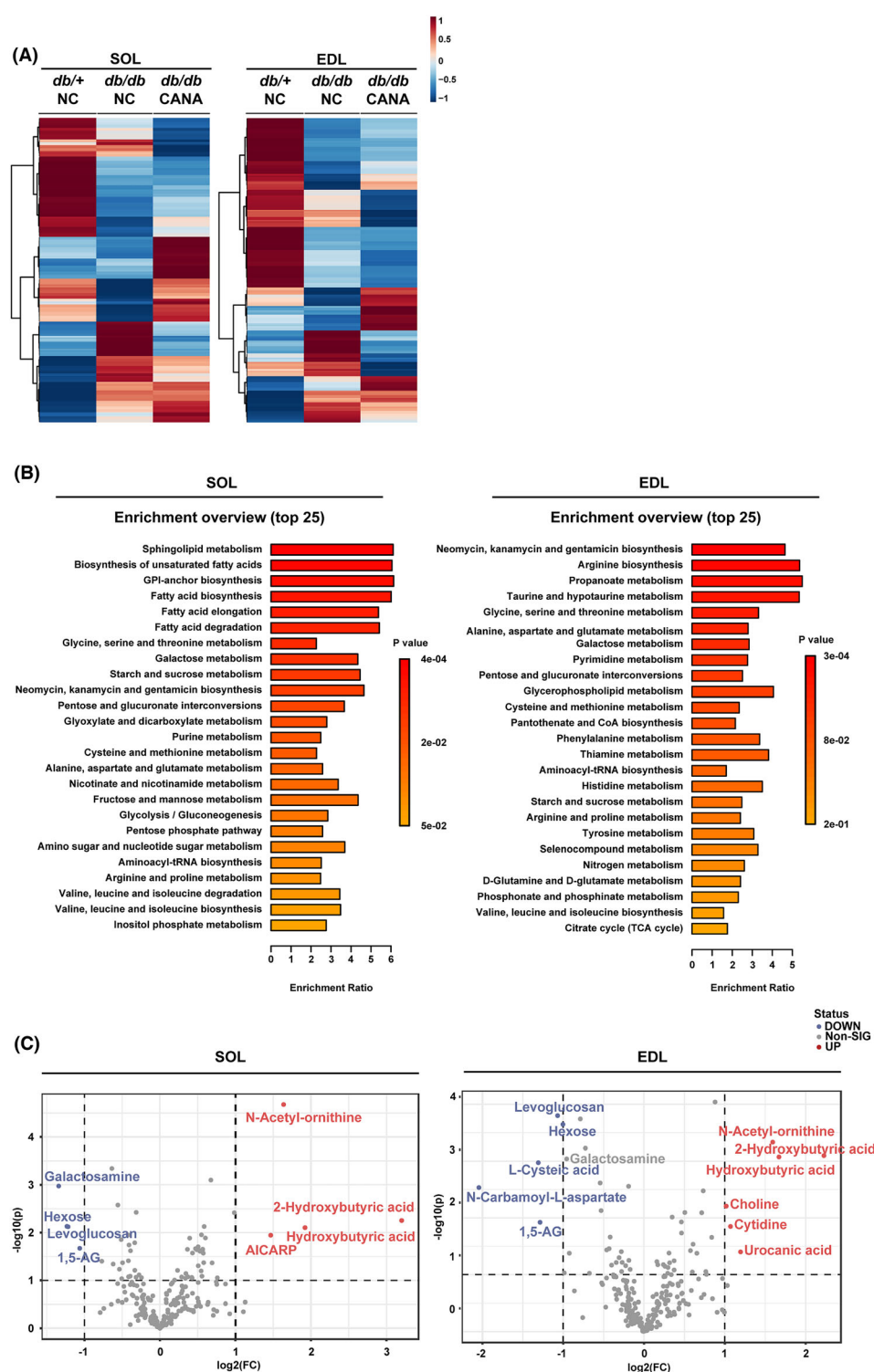
Figure 3 Metabolome analysis of skeletal muscles. (A) Soleus (SOL) and extensor digitorum longus (EDL) from *db/+*, *db/db* and canagliflozin (CANA)-treated *db/db* mouse groups (*n* = 4, each group) were clustered based on metabolomics data (rows). Clustering results shown as a heatmap (distance measure using Euclidean and clustering algorithm using ward.D). Each column represents the mean hydrophilic metabolite from four mice, where red indicates high metabolite level and blue indicates low metabolite level within the three groups. The scale bar indicates *z*-score values, which are calculated by subtracting the mean peak intensity of metabolites across all samples from the individual peak intensity of a specific metabolite and then dividing the result by the standard deviation. (B) Top 25 enriched metabolic pathways affected by CANA treatment in SOL and EDL. (C) Volcano plot representation of hydrophilic metabolites that were significantly changed in SOL and EDL from CANA-treated *db/db* mice. The dotted horizontal line represents the significance threshold (Student's *t* test, $P < 0.05$ vs. control *db/db* mice, *n* = 4).
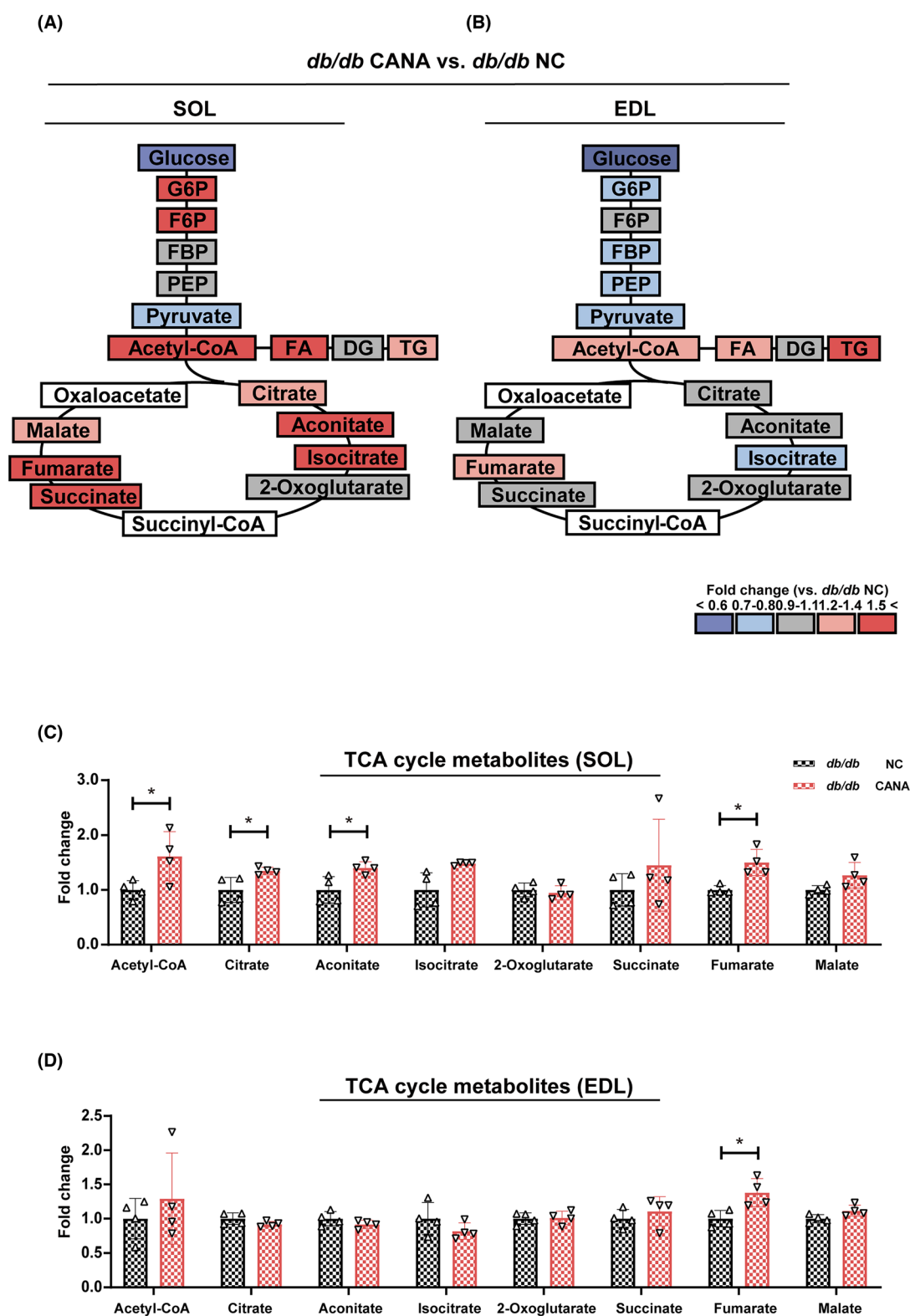
Figure 4 Glycolysis and tricarboxylic acid (TCA) cycle in skeletal muscles. Ratio of metabolites in canagliflozin (CANA)-treated *db/db* mice to control *db/db* mice in soleus (SOL) (A) and extensor digitorum longus (EDL) (B), calculated as fold change. Dark red indicates metabolites with fold change ≥1.5, and dark blue indicates those with fold change ≤0.6. Grey indicates those with no difference between the CANA-treated and control *db/db* mice. White indicates those undetected. Relative metabolite changes in SOL (C) and EDL (D) (*n* = 4). Data are expressed as the mean ± SEM. *$P < 0.05$ versus control *db/db* mice (Student's *t* test).
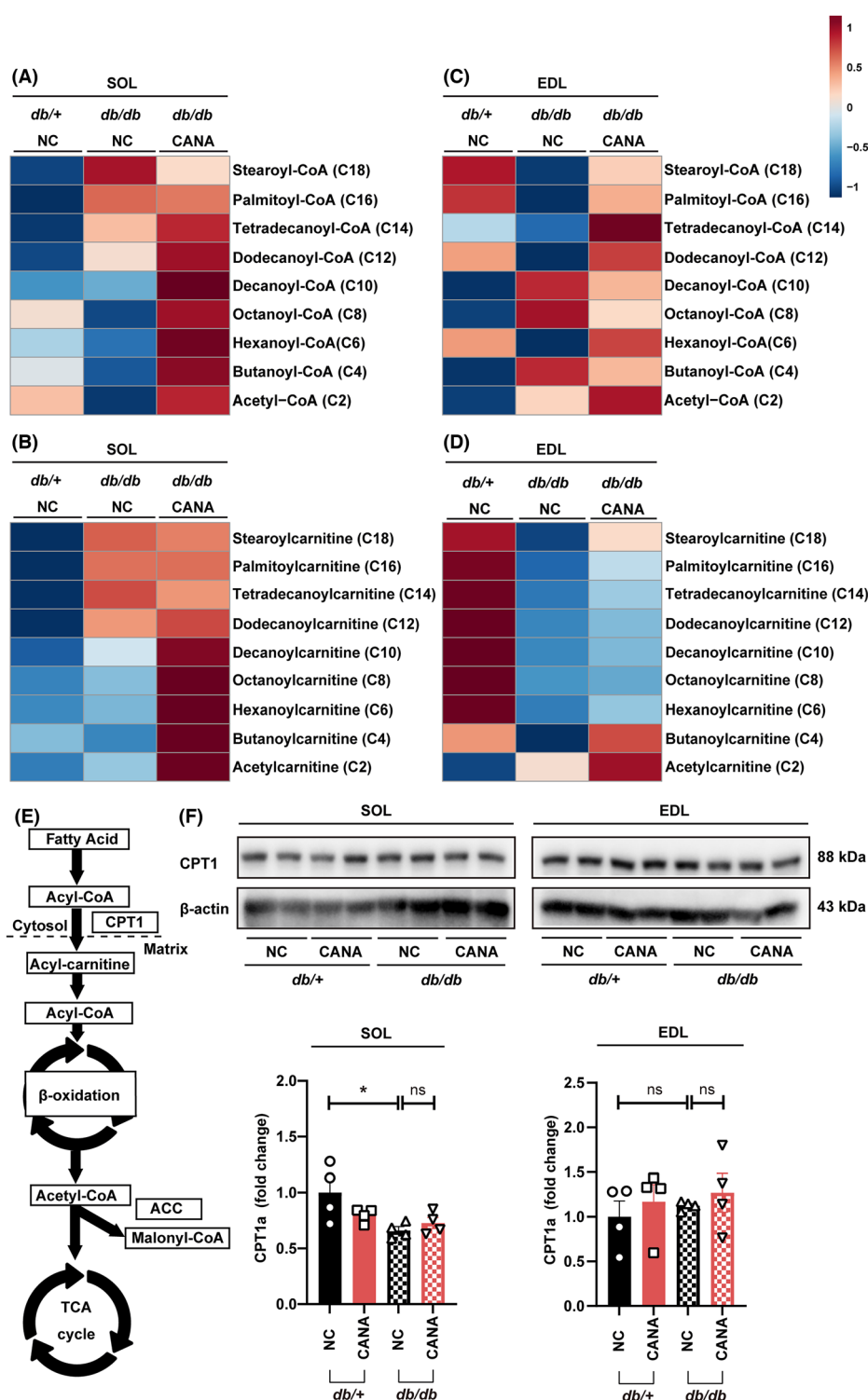
Figure 5 Assessment of metabolites and key enzyme related to fatty acid oxidation in skeletal muscles. (A–D) Heatmap of relative acyl-CoA and acyl-carnitine levels in skeletal muscles from db/+, db/db and canagliflozin (CANA)-treated db/db mice. Each column represents the mean metabolite from four mice, where red indicates high metabolite level and blue indicates low metabolite level within the three mouse groups. Relative acyl-CoA (A) and acyl-carnitine (B) levels in soleus (SOL). Relative acyl-CoA (C) and acyl-carnitine (D) levels in extensor digitorum longus (EDL). The scale bar indicates z-score values, which are calculated by subtracting the mean peak intensity of metabolites across all samples from the individual peak intensity of a specific metabolite and then dividing the result by the standard deviation. (E) Schematic of key enzymatic steps in fatty acid oxidation. (F) Representative immunoblot images and quantification of carnitine palmitoyltransferase 1 (CPT1) expression in SOL and EDL. Data are expressed as the mean ± SEM. *$P < 0.05$ (analysis of variance [ANOVA], $n = 4$). ns, not significant.

Increased mitochondrial FA oxidation is a source of reactive oxygen species (ROS) production. We measured TBARS of oxidative and glycolytic muscles to assess mitochondrial ROS in skeletal muscle.[21] *Db/db* mice had higher TBARS levels in tibialis anterior than *db/+* mice; however, CANA did not affect TBARS levels in oxidative and glycolytic muscles (*Figure S5C*). Furthermore, *db/db* mice had lower GSH levels and higher ratio of oxidized glutathione (GSSG) to GSH in EDL than *db/+* mice. However, CANA did not affect GSH and GSSG/GSH in soleus and EDL muscles from *db/db* mice (*Figure S5D*).

Changes in amino acids in skeletal muscles and blood serum

We previously reported marked changes in amino acids, particularly branched-chain amino acids (BCAAs) in EDL muscle from normoglycaemic mice after CANA treatment.[11] In this study, the levels of BCAAs, such as valine, leucine and isoleucine, increased in soleus and EDL muscles from *db/db* mice, whereas CANA treatment attenuated the increase in valine and leucine (*Figure 6A,B*). We further investigated the metabolites in serum samples from the same mice. The levels of BCAAs and other amino acids, such as lysine, phenylalanine and alanine, were higher in the sera from *db/db* mice than those from *db/+* mice, and these levels were reduced by CANA treatment (*Figure 6C*).

AICARP/AMPK pathway in oxidative soleus muscle

Exogenous administration of AICAR, a dephosphorylated precursor of AICARP, improves endurance capacity through AMP-activated protein kinase (AMPK)-activated FA oxidation in skeletal muscles.[22,23] We, therefore, focused on AICARP as a mechanistic link between the improved endurance capacity and changes in FA oxidation in soleus muscle from *db/db* mice during SGLT2 inhibition. AICARP levels increased ~3-fold in soleus muscle after CANA treatment and were undetectable in serum (*Figures 7A* and *S5E*). Consistently, CANA treatment attenuated the reduction in phosphorylated AMPK in soleus muscle with no increase in AMP/ATP ratios (*Figure 7B,C*). By contrast, there was no significant change in AICARP levels, AMP/ATP ratios and AMPK phosphorylation in EDL muscle from *db/db* mice after CANA treatment (*Figure 7A,B,D*).

SGLT2 is expressed in the kidneys. Consistently, we did not detect SGLT2 in skeletal muscles and C2C12 cells (*Figure S6A*). However, CANA increased AMPK phosphorylation in C2C12 myoblasts (*Figure S6B*). To examine whether CANA directly activates AMPK via AICARP production, we focused on ADSL, an enzyme that converts succinyl-AICAR (SAICAR) to AICARP. Knockdown of ADSL in C2C12 myoblasts did not decrease

CANA-induced AMPK phosphorylation (*Figure S6C*). Furthermore, CANA did not increase AMPK phosphorylation in differentiated C2C12 myotubes (*Figure S6D*).

Discussion

Diabetes increases the risk for sarcopenia, thereby leading to physical inactivity.[24] Conversely, impaired muscle mass and function might exacerbate glucose metabolism, leading to reduced quality of life in patients with diabetes.[24] Elucidating the effect of SGLT2 inhibition on skeletal muscle metabolism is important to understand how SGLT2 inhibitors should be used for the treatment of patients with type 2 diabetes.

In this study, CANA treatment improved running distance but not grip strength in *db/db* mice. These observations are consistent with previous reports that SGLT2 inhibition and exercise exert additive effects on endurance capacity in STZ-treated mice.[12,13] Given the cardioprotective effects of SGLT2 inhibitors,[25] the CANA-induced increase in running distance may be due, at least in part, to the improvement of cardiopulmonary fitness and oxygen-carrying capacity. However, enhanced FA β-oxidation and subsequent increases in acetyl-CoA and intermediates in the TCA cycle in soleus muscle from CANA-treated *db/db* mice suggested that changes in skeletal muscle metabolism can improve endurance capacity (*Figure 8*). Furthermore, our metabolomics data in skeletal muscles are consistent with a previous report that the SGLT2 inhibitor dapagliflozin increases glucose disposal and lipid oxidation in patients with type 2 diabetes.[26] Taken together, these results suggest that SGLT2 inhibition enhances oxidative muscle function in diabetes, thereby shifting the energy substrate from glucose to lipids.

We previously reported that CANA treatment increased glycolytic metabolites in EDL muscle from normoglycaemic mice.[11] In this study, local glucose levels decreased in soleus and EDL muscles from *db/db* mice after CANA treatment. Given the heterogeneity of fibre types in glucose metabolism,[27] the response to changes in glucose levels may differ between oxidative and glycolytic muscles. In fact, acetyl-CoA and glycolytic intermediates, such as G6P and F6P, increased in glycolytic EDL muscle from obese hyperglycaemic mice. This result is consistent with previous reports demonstrating that glucose oxidation is increased in skeletal muscle from people with insulin resistance and diabetes during fasting.[19,28] However, CANA treatment increased G6P and F6P in the soleus muscle rather than the EDL muscle from *db/db* mice. It has been proposed as the glucose–FA cycle or Randle cycle that preferential FA oxidation inhibit glycolysis in skeletal muscle.[29] Increases in acetyl-CoA and citrate may result in allosteric inhibition of PFKM and PDHα, leading to the accumulation of F6P and pyruvate.[30] Given the marginal changes in G6P and F6P in
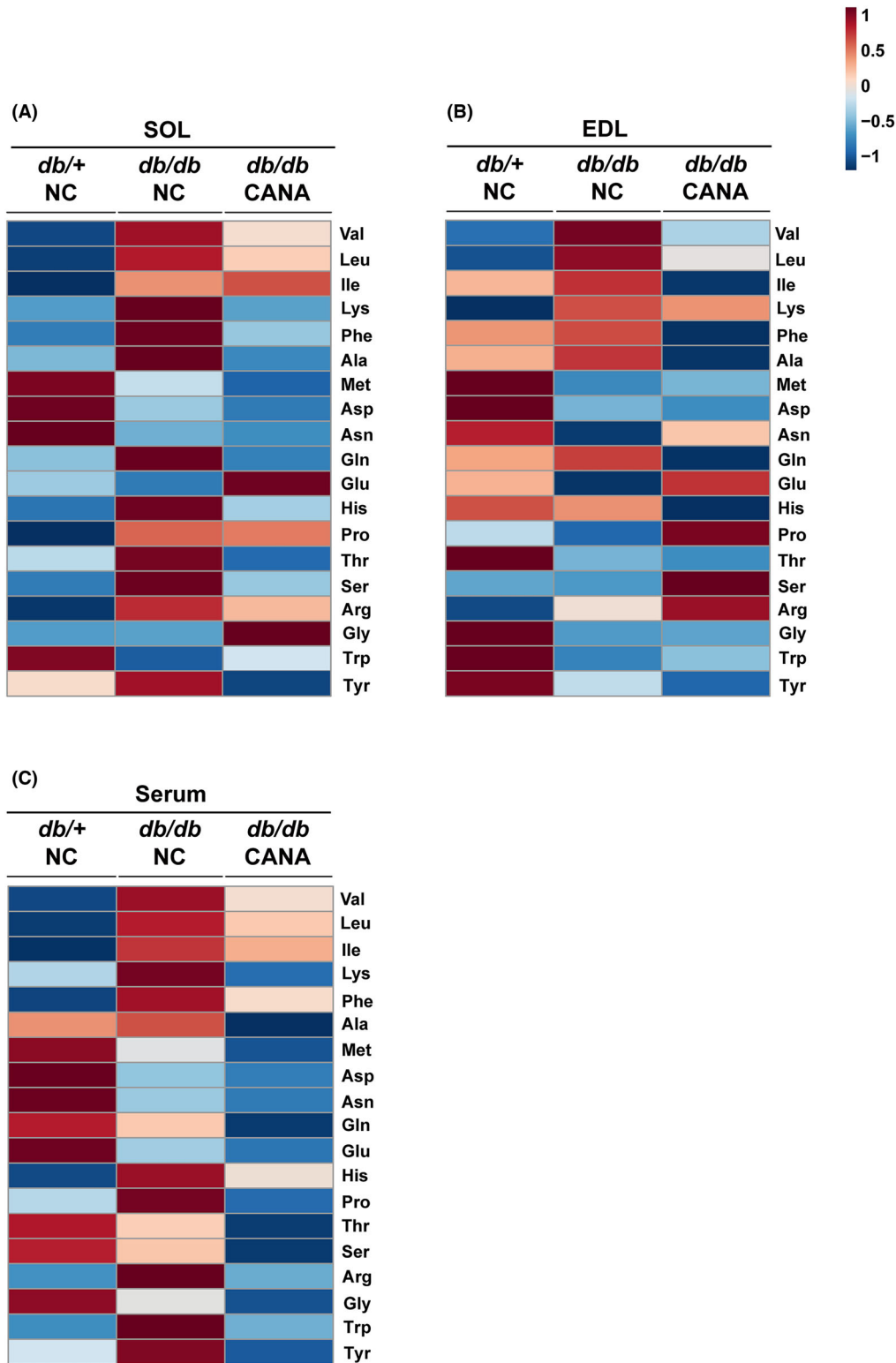
Figure 6 Changes in amino acid levels in skeletal muscles and serum. Heatmap of relative amino acid levels in soleus (SOL) (A) and extensor digitorum longus (EDL) (B) muscles and serum (C) from *db/+*, *db/db* and canagliflozin (CANA)-treated *db/db* mice (*n* = 4). The scale bar indicates *z*-score values, which are calculated by subtracting the mean peak intensity of metabolites across all samples from the individual peak intensity of a specific metabolite and then dividing the result by the standard deviation. Ala, alanine; Arg, arginine; Asn, asparagine; Asp, aspartic acid; Gln, glutamine; Glu, glutamic acid; Gly, glycine; His, histidine; Ile, isoleucine; Leu, leucine; Lys, lysine; Met, methionine; Phe, phenylalanine; Pro, proline; Ser, serine; Thr, threonine; Trp, tryptophan; Tyr, tyrosine; Val, valine.
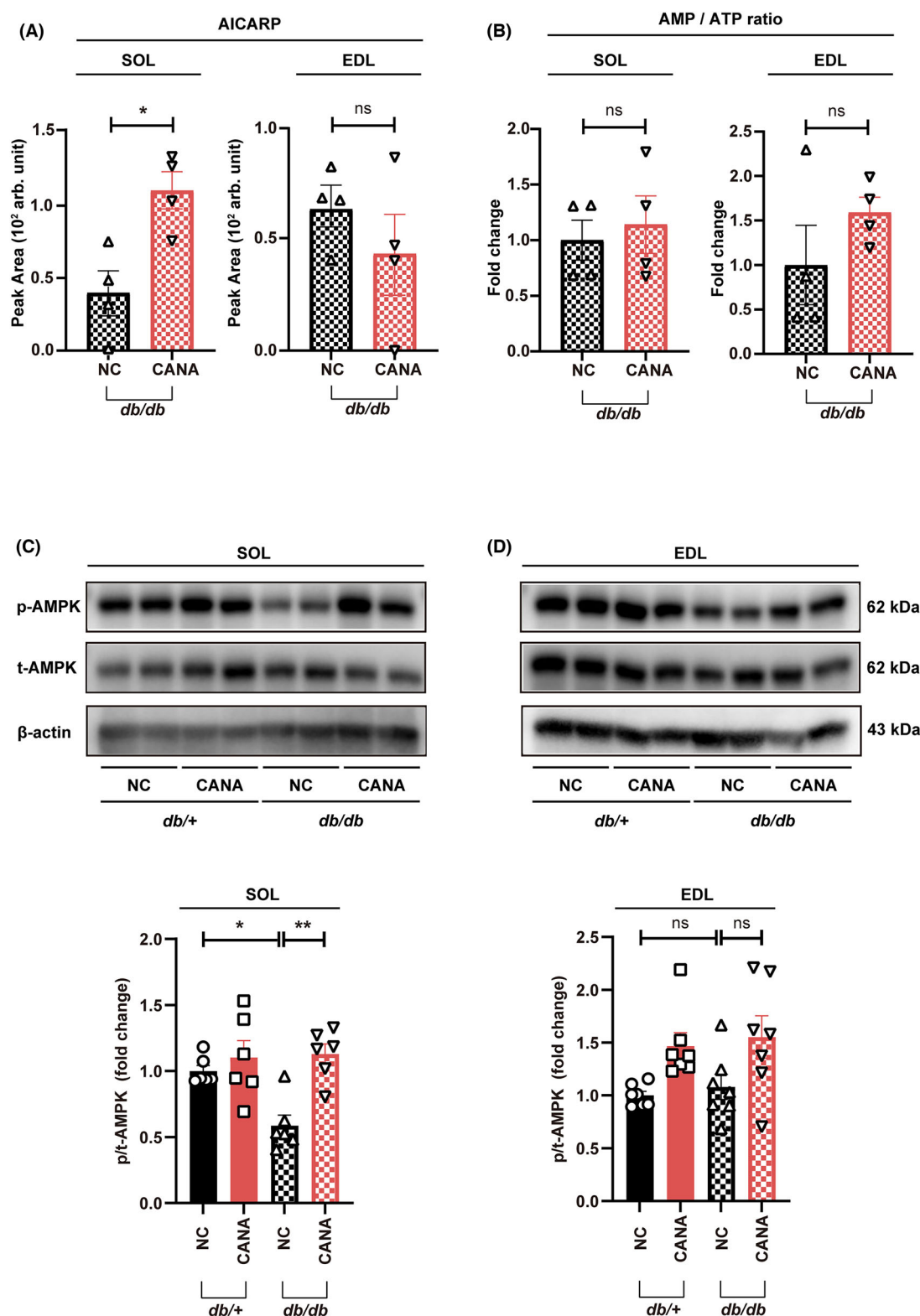
Figure 7 Changes in 5-aminoimidazole-4-carboxamide-1-β-D-ribofuranosyl 5'-monophosphate (AICARP) levels and AMP-activated protein kinase (AMPK) phosphorylation in skeletal muscles. AICARP peak areas (A) and relative AMP/ATP ratios (B) in soleus (SOL) and extensor digitorum longus (EDL) after canagliflozin (CANA) treatment (n = 4). Representative immunoblot images and quantification for the expression of p-AMPK and t-AMPK in SOL (C) and EDL (D) (n = 7). Data are expressed as the mean ± SEM. Group difference was assessed using Student's t test in (A) and (B) or one-way analysis of variance (ANOVA) in (C) and (D). *$P < 0.05$ and **$P < 0.01$. arb. unit, arbitrary unit; ns, not significant.
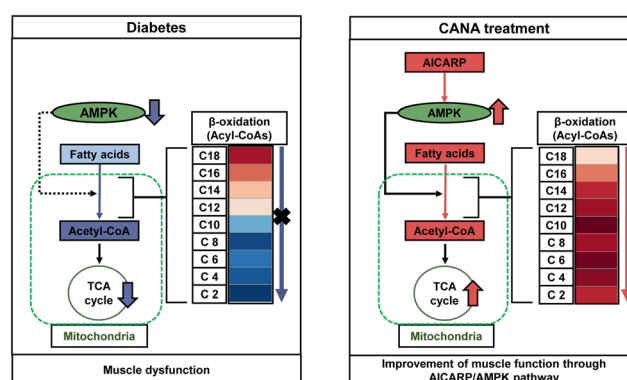
Figure 8 Schematic of major metabolites and 5-aminoimidazole-4-carboxamide-1-β-D-ribofuranosyl 5'-monophosphate (AICARP)/AMP-activated protein kinase (AMPK) pathway in soleus muscle from *db/db* mice. The colours of metabolites are described in *Figures 3* and *4*. Long-chain acyl-CoAs (C12–C18) accumulated in soleus muscle from *db/db* mice, partly because of reduced AMPK activation. Impaired fatty oxidation reduced energy production by the mitochondria and caused muscle dysfunction, such as reduced endurance. Canagliflozin (CANA) treatment induced AICARP accumulation in soleus muscle from *db/db* mice, leading to AMPK activation. AMPK activation enhanced fatty acid β-oxidation in soleus muscle from *db/db* mice, which consequently improved their endurance capacity.

EDL muscle after CANA treatment, whether FA oxidation inhibits glycolysis may depend on muscle characteristics (i.e., glycolytic or oxidative).[31]

In addition to glucose-lowering effect, metabolic changes caused by CANA include an increase in ketones. Ketones are an energy source in skeletal muscle during exercise.[32] In this study, CANA increased 3-hydroxybutyric acid levels in soleus muscle from *db/db* mice. Given the metabolic characteristics of oxidative and glycolytic fibres, ketone utilization may preferentially occur in oxidative muscle during exercise.

Insulin resistance and type 2 diabetes are associated with impaired FA β-oxidation in skeletal muscle.[19,28] Activation of AMPK in skeletal muscle enhances glucose uptake and FA β-oxidation, thereby improving exercise performance.[22,23] In this study, CANA treatment activated AMPK in soleus muscle from *db/db* mice. The mechanisms by which AMPK is activated in skeletal muscle during SGLT2 inhibition remain to be elucidated. Although AMPK is activated by a high AMP/ATP ratio, there are no appreciable changes in the AMP/ATP ratios and AMP levels in soleus and EDL muscles after CANA treatment. Given that SGLT2 inhibitors act primarily on the kidneys, their metabolic impact on skeletal muscle should be indirect.[11,33] Although CANA treatment attenuated glucose accumulation in soleus and EDL muscles from *db/db* mice, there was no significant increase in AMPK activation in the EDL muscle. It is, therefore, interesting to elucidate how the AICRAP/AMPK pathway is activated in oxidative but not in glycolytic muscles, after systemic glycaemic control has been improved in *db/db* mice during SGLT2 inhibition. On the other hand, CANA directly activates AMPK in C2C12 myoblasts independent of AICARP production. Although CANA did not activate AMPK in differentiated C2C12 myotubes, it may act directly on skeletal muscle and enhance FA β-oxidation via AMPK activation.

AICARP is an intermediate in purine metabolism and directly binds to γ subunit of AMPK.[34] Similarly, AICAR, a precursor of AICARP, can increase AMPK phosphorylation (Thr172) by binding to the γ2 subunit of AMPK without changing the ADP/ATP ratio.[35] In this study, CANA treatment increased AICARP levels and AMPK phosphorylation, with increases in medium- to short-chain acyl-CoAs and acyl-carnitines in soleus muscle from *db/db* mice. These observations suggest that AICARP, when induced by CANA treatment, activates AMPK in soleus muscle, leading to increased FA β-oxidation (*Figure 8*). Recent evidence has suggested that exercise induces AICARP accumulation followed by AMPK activation in skeletal muscles,[36] although how AICARP accumulates during SGLT2 inhibition is currently unclear. In the purine de novo synthesis pathway, AICARP is synthesized from SAICAR and is converted into formyl-AICAR (FAICAR). In this study, G6P accumulated in soleus muscle from *db/db* mice after CANA treatment. Thus, G6P possibly flows through the pentose phosphate pathway, followed by the supply of ribose-5-phosphate and 5-phosphoribosylpyrophosphate, which purine synthesis pathway begins with. Further studies are required to elucidate whether AICARP accumulation is causally related to increased G6P levels via purine synthesis in soleus muscle in response to SGLT2 inhibition.

The mechanism of the CANA-induced activation of the AICARP/AMPK pathway in oxidative muscle is unclear. Muscle fibres have different characteristics in purine metabolism, including de novo synthesis and salvage.[37] Although AICARP and AMP have similarities as purine metabolites in activating AMPK, AMP levels are determined in a complex manner. AMP is converted from adenine and adenosine in the salvage pathway in addition to purine synthesis. Therefore, AICARP levels can be increased in oxidative muscle without changing AMP levels.

Although soleus muscle plays an important role in endurance capacity, glycolytic muscles, including gastrocnemius, are also involved in endurance exercise.[38] In this study, the

weight of oxidative soleus muscle from *db/db* mice was unchanged after CANA treatment, whereas the weight of glycolytic muscles such as gastrocnemius and tibialis anterior increased. Therefore, an increase in glycolytic muscle weight may contribute to the improved endurance capacity of *db/db* mice. Furthermore, given that AICAR-induced AMPK activation inhibited protein synthesis,[39] the lack of soleus muscle weight recovery after CANA treatment may be partly due to decreased protein synthesis.

It is important to determine whether CANA affects muscle function through increased physical activity or through CANA-induced metabolic changes. Although CANA-treated mice had normal running behaviour,[12] we cannot exclude the possibility that the activation of the AICARP/AMPK pathway in skeletal muscle is due to increased physical activity in *db/db* mice after CANA treatment. In addition to exercise, methotrexate activates the AICARP/AMPK pathway in skeletal muscle.[40] Methotrexate inhibits the activity of AICAR transformylase/inosine monophosphate cyclohydrolase (ATIC), an enzyme that converts AICARP to FAICAR. It is unclear whether CANA increases AICARP levels in skeletal muscle by inhibiting the enzymatic activity of ATIC. Further studies are required to evaluate whether metabolites such as SAICAR and FAICAR change in the purine synthesis pathway after CANA treatment.

In conclusion, this study provides evidence for the potential role of the AICARP/AMPK pathway in oxidative muscles during SGLT2 inhibition. Our data suggest that SGLT2 inhibition has a potential to improve endurance capacity in patients with type 2 diabetes.

Acknowledgements

Funding information

Conflict of interest statement

Online supplementary material

Additional supporting information may be found online in the Supporting Information section at the end of the article.

References

1. Cruz-Jentoft AJ, Bahat G, Bauer J, Boirie Y, Bruyere O, Cederholm T, et al. Sarcopenia: revised European consensus on definition and diagnosis. *Age Ageing* 2019;**48**:16–31.
2. Mårin P, Andersson B, Krotkiewski M, Björntorp P. Muscle fiber composition and capillary density in women and men with NIDDM. *Diabetes Care* 1994;**17**:382–386.
3. Wang YX, Zhang CL, Yu RT, Cho HK, Nelson MC, Bayuga-Ocampo CR, et al. Regulation of muscle fiber type and running endurance by PPARδ. *PLoS Biol* 2004;**2**:e294.
4. Short KR, Vittone JL, Bigelow ML, Proctor DN, Rizza RA, Coenen-Schimke JM, et al. Impact of aerobic exercise training on age-related changes in insulin sensitivity and muscle oxidative capacity. *Diabetes* 2003;**52**:1888–1896.
5. Baskin KK, Winders BR, Olson EN. Muscle as a "mediator" of systemic metabolism. *Cell Metab* 2015;**21**:237–248.
6. Morrato EH, Hill JO, Wyatt HR, Ghushchyan V, Sullivan PW. Physical activity in U.S. adults with diabetes and at risk for developing diabetes, 2003. *Diabetes Care* 2007;**30**:203–209.
7. Nadeau KJ, Zeitler PS, Bauer TA, Brown MS, Dorosz JL, Draznin B, et al. Insulin resistance in adolescents with type 2 diabetes is associated with impaired exercise capacity. *J Clin Endocrinol Metab* 2009;**94**:3687–3695.
8. Mensink M, Hesselink MKC, Russell AP, Schaart G, Sels JP, Schrauwen P. Improved skeletal muscle oxidative enzyme activity and restoration of PGC-1α and PPARβ/δ gene expression upon rosiglitazone treatment in obese patients with type 2 diabetes mellitus. *Int J Obes (Lond)* 2007;**31**:1302–1310.
9. Obata A, Kubota N, Kubota T, Iwamoto M, Sato H, Sakurai Y, et al. Tofogliflozin improves insulin resistance in skeletal muscle and accelerates lipolysis in adipose tissue in male mice. *Endocrinology* 2016;**157**:1029–1042.
10. Nambu H, Takada S, Fukushima A, Matsumoto J, Kakutani N, Maekawa S,

et al. Empagliflozin restores lowered exercise endurance capacity via the activation of skeletal muscle fatty acid oxidation in a murine model of heart failure. *Eur J Pharmacol* 2020;**866**:172810.

11. Otsuka H, Yokomizo H, Nakamura S, Izumi Y, Takahashi M, Obara S, et al. Differential effect of canagliflozin, a sodium–glucose cotransporter 2 (SGLT2) inhibitor, on slow and fast skeletal muscles from nondiabetic mice. *Biochem J* 2022;**479**:425–444.

12. MacDonald TL, Pattamaprapanont P, Cooney EM, Nava RC, Mitri J, Hafida S, et al. Canagliflozin prevents hyperglycemia-associated muscle extracellular matrix accumulation and improves the adaptive response to aerobic exercise. *Diabetes* 2022;**71**:881–893.

13. Linden MA, Ross TT, Beebe DA, Gorgoglione MF, Hamilton KL, Miller BF, et al. The combination of exercise training and sodium-glucose cotransporter-2 inhibition improves glucose tolerance and exercise capacity in a rodent model of type 2 diabetes. *Metabolism* 2019;**97**:68–80.

14. Bligh EG, Dyer WJ. A rapid method of total lipid extraction and purification. *Can J Biochem Physiol* 1959;**37**:911–917.

15. Fushimi T, Izumi Y, Takahashi M, Hata K, Murano Y, Bamba T. Dynamic metabolome analysis reveals the metabolic fate of medium-chain fatty acids in AML12 cells. *J Agric Food Chem* 2020;**68**:11997–12010.

16. Takeda H, Izumi Y, Takahashi M, Paxton T, Tamura S, Koike T, et al. Widely-targeted quantitative lipidomics method by supercritical fluid chromatography triple quadrupole mass spectrometry. *J Lipid Res* 2018; **59**:1283–1293.

17. Schiaffino S, Reggiani C. Fiber types in mammalian skeletal muscles. *Physiol Rev* 2011;**91**:1447–1531.

18. Petersen KF, Dufour S, Befroy D, Garcia R, Shulman GI. Impaired mitochondrial activity in the insulin-resistant offspring of patients with type 2 diabetes. *N Engl J Med* 2004;**350**:664–671.

19. Kelley DE, Simoneau JA. Impaired free fatty acid utilization by skeletal muscle in non-insulin-dependent diabetes mellitus. *J Clin Invest* 1994;**94**:2349–2356.

20. Abu-Elheiga L, Matzuk MM, Abo-Hashema KA, Wakil SJ. Continuous fatty acid oxidation and reduced fat storage in mice lacking acetyl-CoA carboxylase 2. *Science* 2001;**291**:2613–2616.

21. Jing E, Emanuelli B, Hirschey MD, Boucher J, Lee KY, Lombard D, et al. Sirtuin-3 (Sirt3) regulates skeletal muscle metabolism and insulin signaling via altered mitochondrial oxidation and reactive oxygen species production. *Proc Natl Acad Sci U S A* 2011;**108**: 14608–14613.

22. Narkar VA, Downes M, Yu RT, Embler E, Wang YX, Banayo E, et al. AMPK and PPARδ agonists are exercise mimetics. *Cell* 2008; **134**:405–415.

23. Merrill GF, Kurth EJ, Hardie DG, Winder WW. AICA riboside increases AMP-activated protein kinase, fatty acid oxidation, and glucose uptake in rat muscle. *Am J Physiol* 1997;**273**:E1107–E1112.

24. Mesinovic J, Zengin A, De Courten B, Ebeling PR, Scott D. Sarcopenia and type 2 diabetes mellitus: a bidirectional relationship. *Diabetes Metab Syndr Obes* 2019;**12**:1057–1072.

25. Lopaschuk GD, Verma S. Mechanisms of cardiovascular benefits of sodium glucose co-transporter 2 (SGLT2) inhibitors: a state-of-the-art review. *JACC Basic Transl Sci* 2020;**5**:632–644.

26. Daniele G, Xiong J, Solis-Herrera C, Merovci A, Eldor R, Tripathy D, et al. Dapagliflozin enhances fat oxidation and ketone production in patients with type 2 diabetes. *Diabetes Care* 2016;**39**:2036–2041.

27. Pataky MW, Wang H, Yu CS, Arias EB, Ploutz-Snyder RJ, Zheng X, et al. High-fat diet-induced insulin resistance in single skeletal muscle fibers is fiber type selective. *Sci Rep* 2017;**7**:13642.

28. Kelley DE, Goodpaster B, Wing RR, Simoneau JA. Skeletal muscle fatty acid metabolism in association with insulin resistance, obesity, and weight loss. *Am J Physiol* 1999;**277**:E1130–E1141.

29. Randle PJ, Garland PB, Hales CN, Newsholme EA. The glucose fatty-acid cycle. Its role in insulin sensitivity and the metabolic disturbances of diabetes mellitus. *Lancet* 1963;**1**:785–789.

30. Hue L, Taegtmeyer H. The Randle cycle revisited: a new head for an old hat. *Am J Physiol Endocrinol Metab* 2009;**297**: E578–E591.

31. Guo Z. Pyruvate dehydrogenase, Randle cycle, and skeletal muscle insulin resistance. *Proc Natl Acad Sci U S A* 2015; **112**:E2854.

32. Evans M, Cogan KE, Egan B. Metabolism of ketone bodies during exercise and training: physiological basis for exogenous supplementation. *J Physiol* 2017;**595**: 2857–2871.

33. Ohgaki R, Wei L, Yamada K, Hara T, Kuriyama C, Okuda S, et al. Interaction of the sodium/glucose cotransporter (SGLT) 2 inhibitor canagliflozin with SGLT1 and SGLT2: inhibition kinetics, sidedness of action, and transporter-associated incorporation accounting for its pharmacodynamic and pharmacokinetic features. *J Pharmacol Exp Ther* 2016;**358**:94–102.

34. Steinberg GR, Carling D. AMP-activated protein kinase: the current landscape for drug development. *Nat Rev Drug Discov* 2019;**18**:527–551.

35. Hawley SA, Ross FA, Chevtzoff C, Green KA, Evans A, Fogarty S, et al. Use of cells expressing γ subunit variants to identify diverse mechanisms of AMPK activation. *Cell Metab* 2010;**11**:554–565.

36. Ezagouri S, Zwighaft Z, Sobel J, Baillieul S, Doutreleau S, Ladeix B, et al. Physiological and molecular dissection of daily variance in exercise capacity. *Cell Metab* 2019;**30**: 78–91.e4.

37. Luo L, Ma W, Liang K, Wang Y, Su J, Liu R, et al. Spatial metabolomics reveals skeletal myofiber subtypes. *Sci Adv* 2023;**9**: eadd0455.

38. Fitts RH, Booth FW, Winder WW, Holloszy JO. Skeletal muscle respiratory capacity, endurance, and glycogen utilization. *Am J Physiol* 1975;**228**:1029–1033.

39. Bolster DR, Crozier SJ, Kimball SR, Jefferson LS. AMP-activated protein kinase suppresses protein synthesis in rat skeletal muscle through down-regulated mammalian target of rapamycin (mTOR) signaling. *J Biol Chem* 2002;**277**:23977–23980.

40. Pirkmajer S, Kulkarni SS, Tom RZ, Ross FA, Hawley SA, Hardie DG, et al. Methotrexate promotes glucose uptake and lipid oxidation in skeletal muscle via AMPK activation. *Diabetes* 2015;**64**:360–369.